CFD Code V&V: 2D NACA 0012 in Stall

Vérification et Validation en Modélisation Numérique

Project

David Vidal

S. Paquette-Greenbaum, R. Zachariah, & K. A. N. Lippert

April 19th 2024

https://github.com/karolali22/MEC8211_PROJECT

POLYTECHNIQUE
MONTRÉAL

MODEL

This V&V procedure makes use of the Chapel-Multiphysics (CHAMPS) in-house CFD code. CHAMPS is a CFD code developed in Eric Laurendeau's laboratory. Eric Laurendeau is professor at Polytechnique Montréal in the Department of Mechanical Engineering. The Unsteady Reynolds Averaged Navier-Stokes (URANS) equations are solved in this procedure to determine the model's adequacy in the context of a reference case described in:

- C. L. Ladson, "NASA Technical Memorandum 4074: Effects of independent variation of Mach and Reynolds numbers on the low-speed aerodynamic characteristics of the NACA 0012 airfoil section", 1988. [Online]. Available: https://api.semanticscholar.org/CorpusID:117770433

The model utilized in the V&V procedure is configured as follows to solve the URANS equations:

- Convective scheme: 1^{st} – order upwind Roe scheme (Flux-Difference Splitting)
- Turbulent viscosity model: Spalart-Allmaras model
- Temporal scheme: Time-Spectral method (Fourier series to transform the URANS equations into a steady problem in the frequency domain)
- Convergence criteria: 10^{-5} for density
- Mesh: O-meshes with varying mesh refinement, viscous wall and farfield boundary conditions

The selected experimental reference case has the following nominal parameters:

- Geometry: NACA 0012 airfoil
- Reynolds number: $Re = 5.970 \times 10^6$
- Mach number: $M = 0.15$
- Angle of attack: α = [-4.05, -2.00, 0.05, 1.98, 4.18, 6.20, 8.22, 10.18, 11.08, 12.25, 13.10, 14.28, 15.20, 16.18, 16.9, 17.35, 17.65, 18.65]°
- Surface roughness: $\varepsilon = 0$

MATHEMATICAL EQUATIONS

1 Navier-Stokes Equations

For compressible and viscous flow, the Navier-Stokes continuity, momentum, and energy equations are respectively defined as follows:

$$\frac{\partial \rho}{\partial t} + \nabla \cdot (\rho \mathbf{u}) = 0 \tag{1}$$

$$\frac{\partial (\rho \mathbf{u})}{\partial t} + \nabla \cdot (\rho \mathbf{u} \otimes \mathbf{u}) = -\nabla p + \nabla \cdot \tau + \rho \mathbf{g} \tag{2}$$

$$\frac{\partial (\rho e)}{\partial t} + \nabla \cdot (\rho \mathbf{u} e) = -\nabla \cdot (p \mathbf{u}) + \nabla \cdot (\tau \cdot \mathbf{u}) - \nabla \cdot \mathbf{q} + \rho \mathbf{g} \cdot \mathbf{u} \tag{3}$$

Where the viscous shear stress tensor τ in a Newtonian fluid is defined as:

$$\tau_{ij} = \mu \left(\frac{\partial u_i}{\partial x_j} + \frac{\partial u_j}{\partial x_i} \right) - \frac{2}{3} \mu \left(\nabla \cdot \mathbf{u} \right) \delta_{ij} \tag{4}$$

CONTINUED: MATHEMATICAL EQUATIONS

2 Reynolds Averaging

Reynolds averaging involves decomposing a flow variable ϕ into its mean $\overline{\phi}$ and fluctuating ϕ' parts:

$$\phi = \overline{\phi} + \phi' \tag{5}$$

Where the time-average of the flow variable ϕ is:

$$\overline{\phi} = \frac{1}{T}\int_{t}^{t+T} \phi \, dt \tag{6}$$

3 RANS

After applying Reynolds' decomposition and time-averaging, the Reynolds Averaged Navier-Stokes continuity, momentum, and energy equations are respectively defined as follows:

$$\frac{\partial \overline{\rho}}{\partial t} + \nabla \cdot (\overline{\rho}\overline{\mathbf{u}}) = 0 \tag{7}$$

$$\frac{\partial (\overline{\rho}\overline{\mathbf{u}})}{\partial t} + \nabla \cdot (\overline{\rho}\overline{\mathbf{u}} \otimes \overline{\mathbf{u}}) = -\nabla \overline{p} + \nabla \cdot (\overline{\tau} + \tau_{\text{turb}}) + \overline{\rho}\mathbf{g} \tag{8}$$

$$\frac{\partial (\overline{\rho e})}{\partial t} + \nabla \cdot (\overline{\rho \mathbf{u} e}) = -\nabla \cdot (\overline{p}\overline{\mathbf{u}}) + \nabla \cdot (\overline{\tau} \cdot \overline{\mathbf{u}}) + \nabla \cdot (\mathbf{q}_{\text{turb}} + \overline{\mathbf{q}}) + \overline{\rho}\mathbf{g} \cdot \overline{\mathbf{u}} \tag{9}$$

CONTINUED: MATHEMATICAL EQUATIONS

4 Spalart–Allmaras Turbulence Model

The Reynolds stress tensor τ_{turb} can be modelled as:

$$\tau_{\text{turb}} = 2\nu_t \overline{S} - \frac{2}{3}\rho k \mathbf{I} \tag{10}$$

Where f_{v1} is a damping function and ν_t is turbulent viscosity:

$$\nu_t = f_{v1}\tilde{\nu} \tag{11}$$

The primary variable of the Spalart-Allmaras model, modified kinematic viscosity $\tilde{\nu}$, is found through its transport equation:

$$\frac{\partial \tilde{\nu}}{\partial t} + \mathbf{u} \cdot \nabla \tilde{\nu} = c_{b1}[1 - f_{t2}]\frac{\tilde{\nu}}{\kappa^2 d^2} S\tilde{\nu} + \frac{1}{\sigma}\left(\nabla \cdot ((\nu + \tilde{\nu})\nabla\tilde{\nu}) + c_{b2}(\nabla\tilde{\nu})^2\right) - c_{w1} f_w \left(\frac{\tilde{\nu}}{d}\right)^2 \tag{12}$$

The definition of the transport equation's parameters and nominal values for its coefficients can be found in:

P. Spalart and S. Allmaras, "A One-Equation Turbulence Model for Aerodynamic Flows," AIAA, vol. 439, Jan. 1992. DOI: 10.2514/6.1992-439.

DISCRETIZATION

1 Roe Scheme: Conservative Laws - Hyperbolic PDE

The Roe scheme's discretization is based on the conservative form of the fluid dynamics equations which can be described as the following in the context of the Euler equations:

$$\frac{\partial \mathbf{U}}{\partial t} + \frac{\partial \mathbf{F}(\mathbf{U})}{\partial x} + \frac{\partial \mathbf{G}(\mathbf{U})}{\partial y} = 0 \tag{1}$$

Where $\mathbf{U}$ is the vector of conservative variables, and $\mathbf{F}(\mathbf{U})$ and $\mathbf{G}(\mathbf{U})$ are the vector of fluxes in the x and y directions:

$$\mathbf{U} = \begin{bmatrix} \rho \\ \rho u \\ \rho v \\ E \end{bmatrix}, \quad \mathbf{F}(\mathbf{U}) = \begin{bmatrix} \rho u \\ \rho u^2 + p \\ \rho uv \\ (E+p)u \end{bmatrix}, \quad \mathbf{G}(\mathbf{U}) = \begin{bmatrix} \rho v \\ \rho uv \\ \rho v^2 + p \\ (E+p)v \end{bmatrix} \tag{2}$$

Closed by the equation of state:

$$p = (\gamma - 1)(E - \frac{1}{2}\rho u^2) \tag{3}$$

$\mathbf{A}(\mathbf{U})$ and $\mathbf{B}(\mathbf{U})$ are the Jacobian matrices in the x and y directions and are given by:

$$\mathbf{A}(\mathbf{U}) = \frac{\partial \mathbf{F}}{\partial \mathbf{U}} = \begin{bmatrix} 0 & 1 & 0 \\ \frac{\gamma-3}{2}u^2 & (3-\gamma)u & \gamma - 1 \\ u\left(\frac{\gamma-2}{2}u^2 - H\right) & H - (\gamma-1)u^2 & \gamma u \end{bmatrix} \tag{4}$$

$$\mathbf{B}(\mathbf{U}) = \frac{\partial \mathbf{G}}{\partial \mathbf{U}} = \begin{bmatrix} 0 & 0 & 1 \\ \frac{\gamma-3}{2}v^2 & \gamma - 1 & (3-\gamma)v \\ v\left(\frac{\gamma-2}{2}v^2 - H\right) & \gamma v & H - (\gamma-1)v^2 \end{bmatrix} \tag{5}$$

Where the enthalpy H is defined as:

$$H = \frac{E+p}{\rho} \tag{6}$$

CONTINUED: DISCRETIZATION

2 Discretization of the Roe Scheme

Flux in the x and y directions can be discretized as the following, where $\mathbf{U}_L$ and $\mathbf{U}_R$ are the states on the left and right sides of a cell interface in the x direction, and where $\mathbf{U}_B$ and $\mathbf{U}_T$ are the states on the bottom and top sides of a cell interface in the y direction:

$$\hat{\mathbf{F}}(\mathbf{U}_L, \mathbf{U}_R) = \frac{1}{2}\left(\mathbf{F}(\mathbf{U}_L) + \mathbf{F}(\mathbf{U}_R)\right) - \frac{1}{2}|\mathbf{A}(\tilde{\mathbf{U}})|(\mathbf{U}_R - \mathbf{U}_L) \tag{7}$$

$$\hat{\mathbf{G}}(\mathbf{U}_B, \mathbf{U}_T) = \frac{1}{2}\left(\mathbf{G}(\mathbf{U}_B) + \mathbf{G}(\mathbf{U}_T)\right) - \frac{1}{2}|\mathbf{B}(\tilde{\mathbf{U}})|(\mathbf{U}_T - \mathbf{U}_B) \tag{8}$$

CONTINUED: DISCRETIZATION

3 Roe Scheme Procedure

1. The Roe-averaged states are computed at the interface of adjacent cells. The Roe-averaged state vector $\tilde{\mathbf{U}}$ must be determined in the x and y direction in order to compute $\mathbf{A}(\tilde{\mathbf{U}})$ and $\mathbf{B}(\tilde{\mathbf{U}})$, where $\mathbf{U}_L$ and $\mathbf{U}_R$ are the states on the left and right sides of a cell interface in the x direction, and where $\mathbf{U}_B$ and $\mathbf{U}_T$ are the states on the bottom and top sides of a cell interface in the y direction:

$$\tilde{\mathbf{U}} = [\tilde{\rho}, \tilde{\rho}\tilde{u}, \tilde{\rho}\tilde{v}, \tilde{E}]^T \tag{9}$$

2. Where $\tilde{\rho}$, $\tilde{\rho}\tilde{u}$, $\tilde{\rho}\tilde{v}$, and $\tilde{E}$ are given by:

$$\tilde{\rho} = \sqrt{\rho_L \rho_R} \quad \text{or} \quad \sqrt{\rho_B \rho_T} \tag{10}$$

$$\tilde{u} = \frac{\sqrt{\rho_L}u_L + \sqrt{\rho_R}u_R}{\sqrt{\rho_L} + \sqrt{\rho_R}}, \quad \tilde{v} = \frac{\sqrt{\rho_B}v_B + \sqrt{\rho_T}v_T}{\sqrt{\rho_B} + \sqrt{\rho_T}} \tag{11}$$

$$\tilde{H} = \frac{\sqrt{\rho_L}H_L + \sqrt{\rho_R}H_R}{\sqrt{\rho_L} + \sqrt{\rho_R}} \quad \text{or} \quad \frac{\sqrt{\rho_B}H_B + \sqrt{\rho_T}H_T}{\sqrt{\rho_B} + \sqrt{\rho_T}} \tag{12}$$

$$\tilde{e} = \tilde{H} - \frac{1}{2}(\tilde{u}^2 + \tilde{v}^2) \tag{13}$$

$$\tilde{E} = \tilde{\rho}\tilde{e} + \frac{1}{2}\tilde{\rho}(\tilde{u}^2 + \tilde{v}^2), \quad \text{where} \quad \tilde{e} = \tilde{H} - \frac{1}{2}(\tilde{u}^2 + \tilde{v}^2) \tag{14}$$

3. The Roe matrices $\mathbf{A}(\tilde{\mathbf{U}})$ and $\mathbf{B}(\tilde{\mathbf{U}})$ can then be computed, allowing the usage of the flux-difference splitting scheme in the x and y directions, where $|\mathbf{A}(\tilde{\mathbf{U}})|$ and $|\mathbf{B}(\tilde{\mathbf{U}})|$ are the absolute values of the Roe matrices' eigenvalues:

$$\hat{\mathbf{F}}(\mathbf{U}_L, \mathbf{U}_R) = \frac{1}{2}\left(\mathbf{F}(\mathbf{U}_L) + \mathbf{F}(\mathbf{U}_R)\right) - \frac{1}{2}|\mathbf{A}(\tilde{\mathbf{U}})|(\mathbf{U}_R - \mathbf{U}_L) \tag{15}$$

$$\hat{\mathbf{G}}(\mathbf{U}_B, \mathbf{U}_T) = \frac{1}{2}\left(\mathbf{G}(\mathbf{U}_B) + \mathbf{G}(\mathbf{U}_T)\right) - \frac{1}{2}|\mathbf{B}(\tilde{\mathbf{U}})|(\mathbf{U}_T - \mathbf{U}_B) \tag{16}$$

4. The computed fluxes can be used to update the conservative variables $\mathbf{U}$ across all cells for a given time step Δt.

CONTINUED: DISCRETIZATION

The Time-Spectral Method is employed to transform the URANS equations into a steady problem in the frequency domain such that the unsteady stall phenomena can be properly captured. This algorithm is described in literature:

- K. C. Hall, J. P. Thomas, and W. S. Clark, "Computation of unsteady nonlinear flows in cascades using a harmonic balance technique," AIAA Journal, vol. 40, no. 5, pp. 879-886, 2002. [Online]. Available: https://doi.org/10.2514/2.1754

- A. Gopinath and A. Jameson, "Time spectral method for periodic unsteady computations over two- and three-dimensional bodies," in AIAA Paper 2005-1220, Jan. 2005. [Online]. Available: https://doi.org/10.2514/6.2005-1220

- M. McMullen, A. Jameson, and J. Alonso, "Application of a non-linear frequency domain solver to the Euler and Navier-Stokes equations," in AIAA Paper 2002-0120, Jan. 2002. [Online]. Available: https://doi.org/10.2514/6.2002-120

CODE VERIFICATION

System Response Quantities for coarse, medium and fine mesh have been recorded for mesh sizes as mentioned below:

- **Coarse Mesh :** 64 x 64
- **Medium Mesh :** 128 x 128
- **Fine Mesh :** 256 x 256

Experimental data obtained for mesh dimension **512 x 512** is considered as the pseudo-analytical solution for code verification. It can be observed that the finer mesh SRQ (256 x 256) is the closest to the pseudo-analytical data. Further analysis shows that the observed order of convergence is in agreement with the formal order of 1.

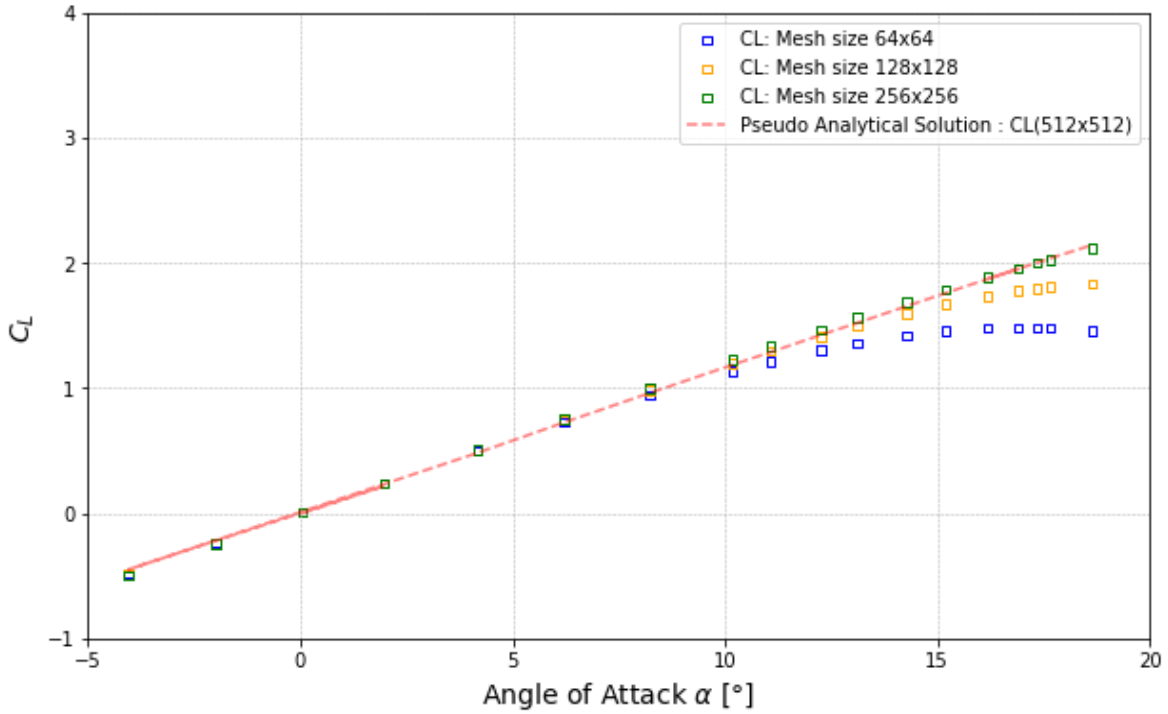

CONTINUED: CODE VERIFICATION

To further verify the code, the observed order of convergence is calculated to evaluate the performance and the reality of the numerical simulation. With the System Response Quantities (SRQ) obtained for the coarse, medium and fine meshes, the L_1 error, L_2 error and L_{inf} error are calculated and used to quantify the discrepancies with respect to the pseudo-analytical solution, 512 x 512 mesh.

To calculate the observed order of convergence, the following equation can be used, where r is the mesh refinement factor:

$$\hat{p} = \frac{\ln\left(\frac{L2_{coarse} - L2_{medium}}{L2_{medium} - L2_{fine}}\right)}{\ln(r)}$$

It can be concluded that the observed order of convergence is 1.0438773935822128. As the observed order of convergence and the formal order of convergence are in agreement, it can be verified that the numerical simulation adapted is accurate and reliable under the given conditions.

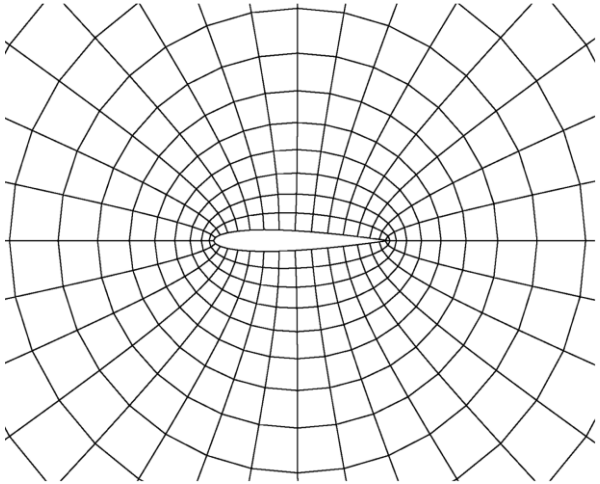

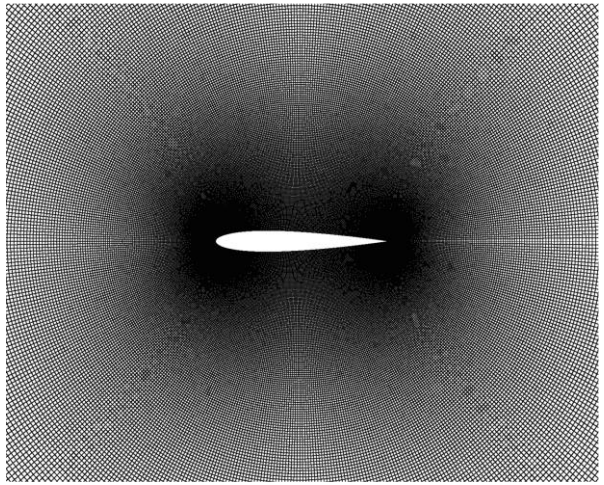

NUMERICAL UNCERTAINTY – u_{num}

The order of convergence is further used to assess the convergence of the simulation with respect to the grid refinement as mentioned before. This is performed to ensure the reliability and accuracy of the simulation results obtained. The GCI can be assessed at each setpoint by determining its respective order of convergence.

The grid convergence equation is calculated using:

$$GCI = \frac{F_s}{r^p - 1}\left|SRQ_{medium} - SRQ_{fine}\right|$$

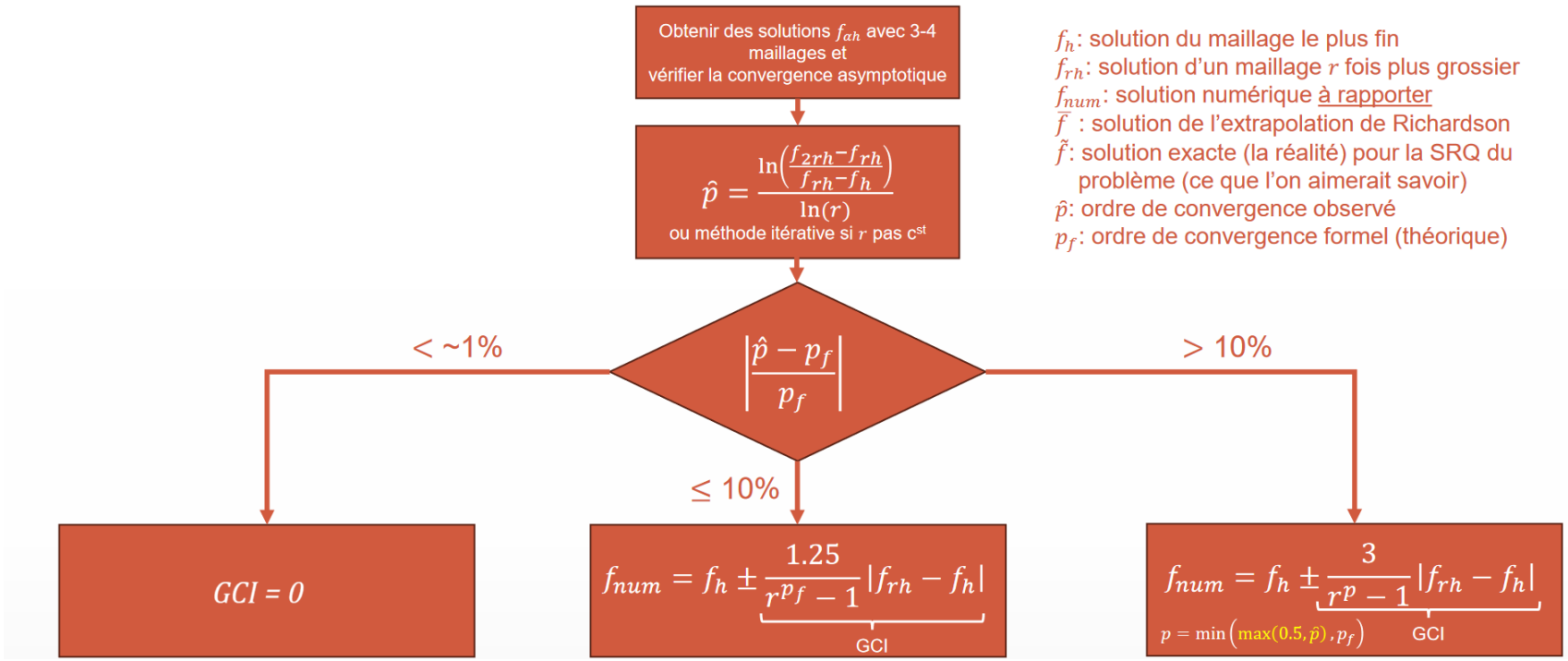

Image 1: GCI Flowchart Summary. *David Vidal*. MEC8211 – Vérification de code.

CONTINUED: NUMERICAL UNCERTAINTY – u_{num}

The variation of GCI in function of setpoint is shown in the figure below. It can be seen that GCI for both C_L and C_D SRQs increase in function of angle of attack. The increase in GCI denotes how well the solution has converged as the grid is refined. The increase in GCI is seen nearer to the region of stall, indicating that there is greater numerical uncertainty at higher angles of attack.

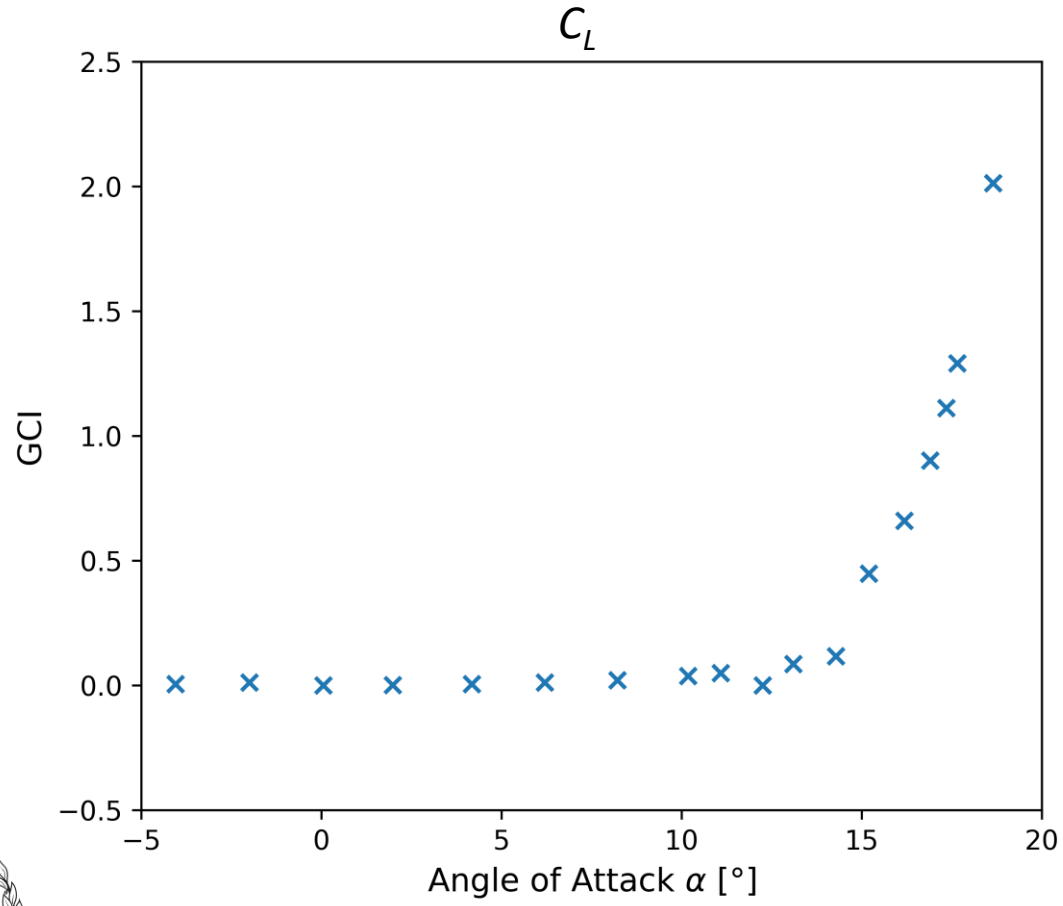

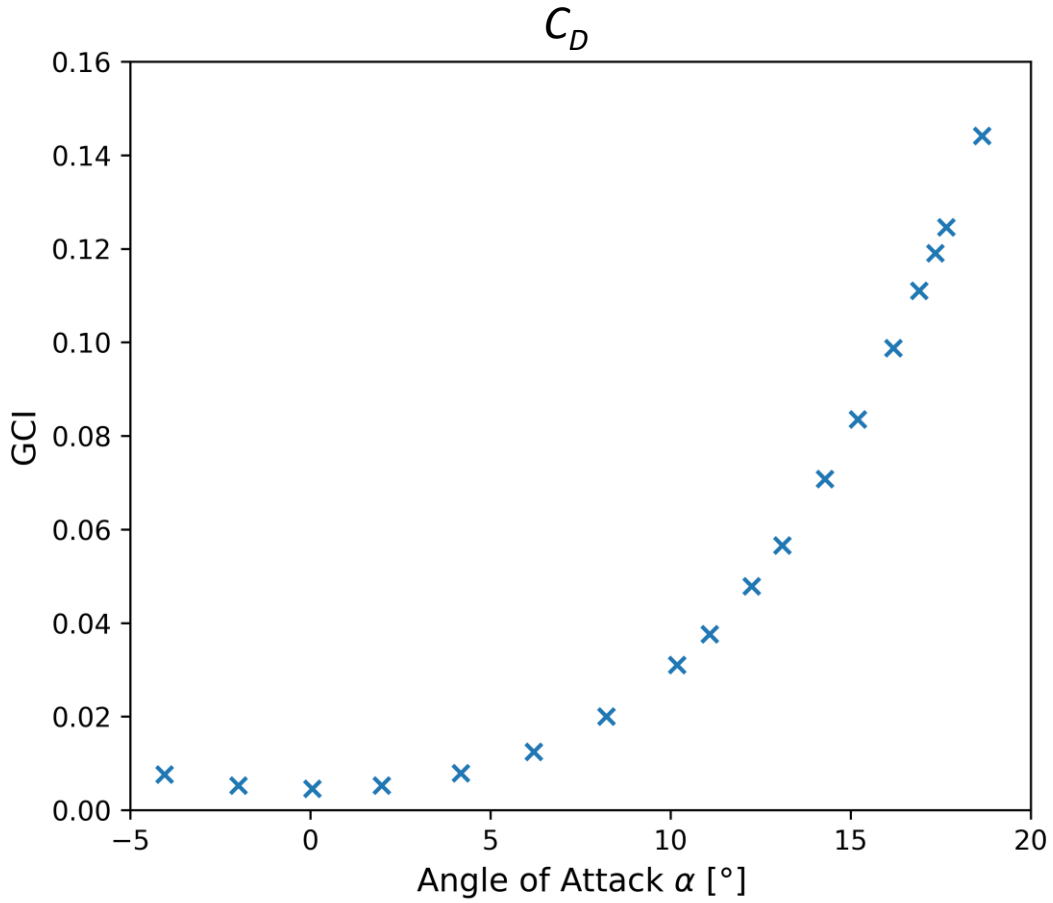

EXPERIMENTAL UNCERTAINTY – u_D

Determining the experimental uncertainty of the SRQs is straightforward as their epistemic uncertainties regarding experimental readings are reported explicitly in the Ladson 1988 experimental reference text. The uncertainties provided are considered to be epistemic as the reference text does not specify the confidence over its reported values.

The reference text makes mention of only 1 epistemic uncertainty per SRQ and does not differ in function of angle of attack. While this may not to be rigorous, the reported uncertainties are taken at face value given their small magnitude with respect to the other sources of uncertainty.

① C_L = ± 0.004
② C_D = ± 0.0002

- Following ASME V&V20, Section 4:

$$u_D = u_r = \sqrt{(b_r^2 + s_r^2)}$$

- For the C_L SRQ:

$$u_D = 0.004$$

- For the C_D SRQ:

$$u_D = 0.0002$$

INPUT UNCERTAINTY – u_{input}

Input uncertainty in this validation procedure is determined via the propagation of uncertainty in the context of a Monte-Carlo Simulation (MCS). The Ladson 1988 experimental reference text does not specify input uncertainties for its experiments. For that reason, input uncertainties are either inferred when possible, or arbitrarily chosen when applicable.

The Langley Research Center is located in Hampton, Virginia, and historically experiences yearly respective high and low temperatures of 31 and 1 °C. The range of possible Reynolds numbers can be inferred from this fact given that wind tunnel apparatus is said to be kept at “near ambient conditions”. Angle of attack and Mach number are arbitrarily chosen to be normally distributed around their means for each setpoint. For simplicity, no uncertainty is attributed to the surface roughness input given its distribution’s log-normal nature. This uncertainty will be included in model error.

① Epistemic uncertainty for Reynolds number: $Re \in [5.591, 6.725] \times 10^6$
② Aleatory uncertainty for Mach number: $M \equiv (\ \mu = 0.15\ \&\ \sigma = 0.015\ )$
③ Aleatory uncertainty for Angle of attack: $\alpha \equiv (\ \mu$ varies with setpoint & $\sigma = 0.75°\ )$
④ No uncertainty for surface roughness: $\varepsilon = 0$

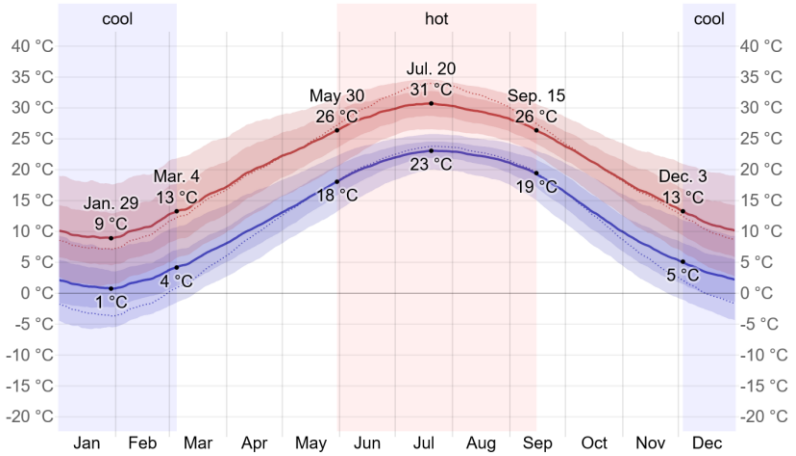

Image 2: Hampton, Virginia Yearly Weather. *WeatherSpark*. https://weatherspark.com

CONTINUED: INPUT UNCERTAINTY – u_{input}

The result of the MCS are mixed aleatory-epistemic distributions given that $Re \in [5.591, 6.725] \times 10^6$. Given the nature of the distributions, a conservative approach is taken to the determination of the input uncertainty for each setpoint. The nominal experimental value for Reynolds number is $Re = 5.970 \times 10^6$. For each angle of attack setpoint, a MCS with 60 samples is conducted for $Re = 5.591 \times 10^6$, 5.970×10^6, and 6.725×10^6. Across the 18 measured setpoints, 3240 simulations were conducted in total. The SRQ mean is taken from the $Re = 5.970 \times 10^6$ MCS, whereas the standard deviations are taken from the lower and upper bounds of the epistemic uncertainty resulting from the range $Re \in [5.591, 6.725] \times 10^6$. The following equation describes the algorithm utilized for determining input uncertainty. Although this approach is conservative, it ensures that the 95.4% confidence interval is respected.

$$u_{input} = \max\left(abs(\mu_{lower} - \mu), abs(\mu_{lower} - \mu)\right) + max\left(\sigma_{lower}, \sigma_{upper}\right)$$

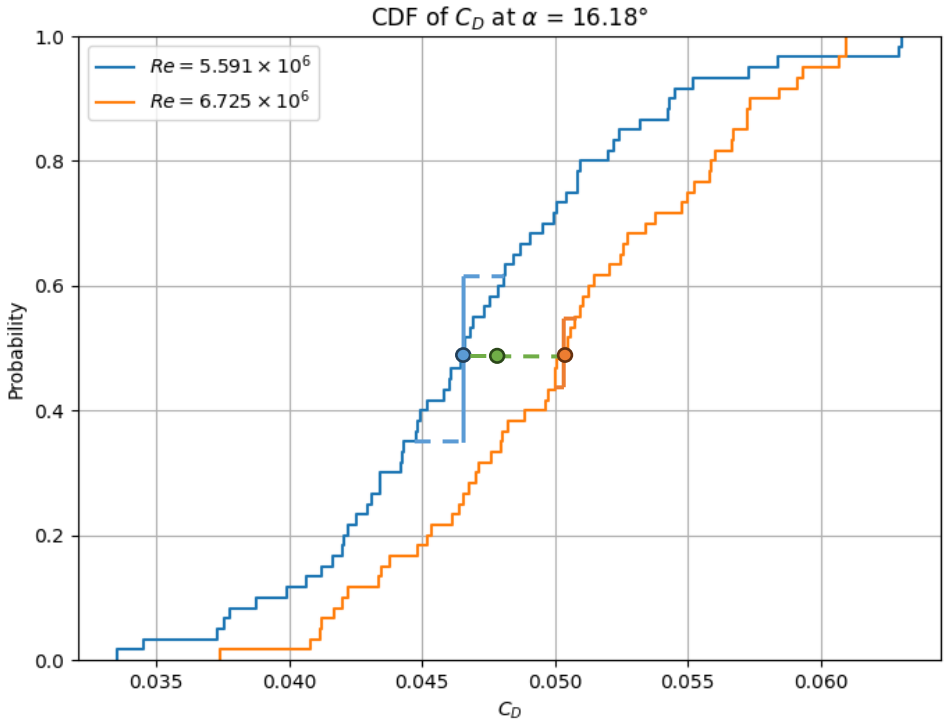

COMPARISON ERROR – E

The experimental SRQs for all setpoints are retrieved from the Ladson 1988 reference text for the flow conditions of M = 0.15, Re = 5.97×10^6, and a free transition airfoil surface roughness. The numerical SRQs are computed with the same Reynolds number and surface roughness, along with a normally distributed Mach number of $\mu = 0.15$ and $\sigma = 0.015$ across 60 samples per setpoint. The mean SQRs are computed for each setpoint.

- Comparison error can be determined by finding the difference between the experimental SRQs and mean simulation SRQs.

$$E = S - D$$

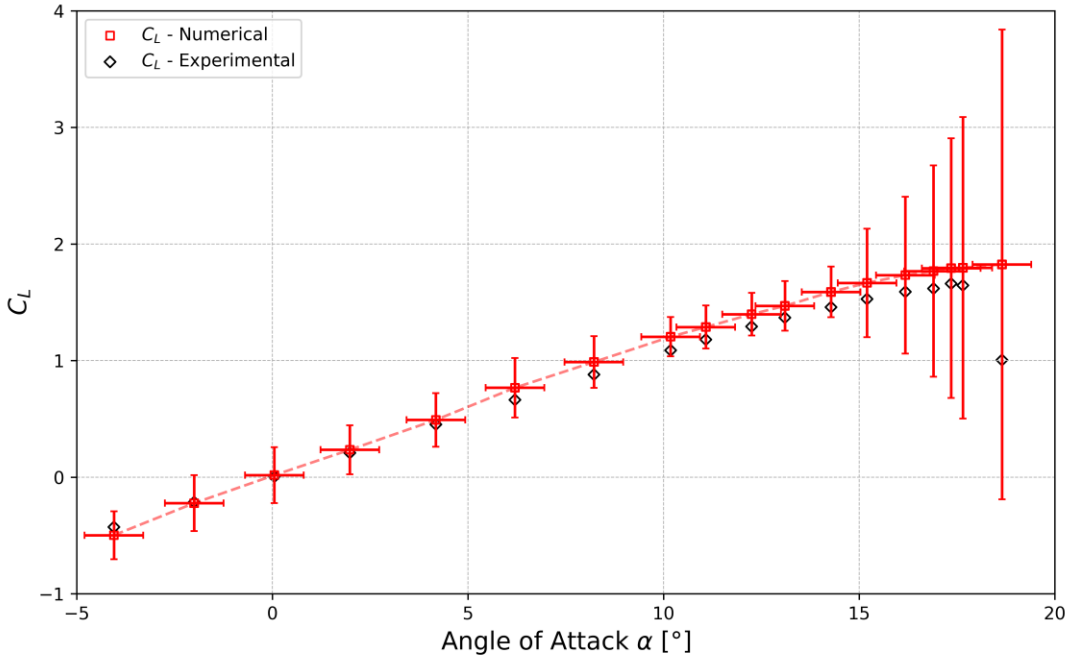

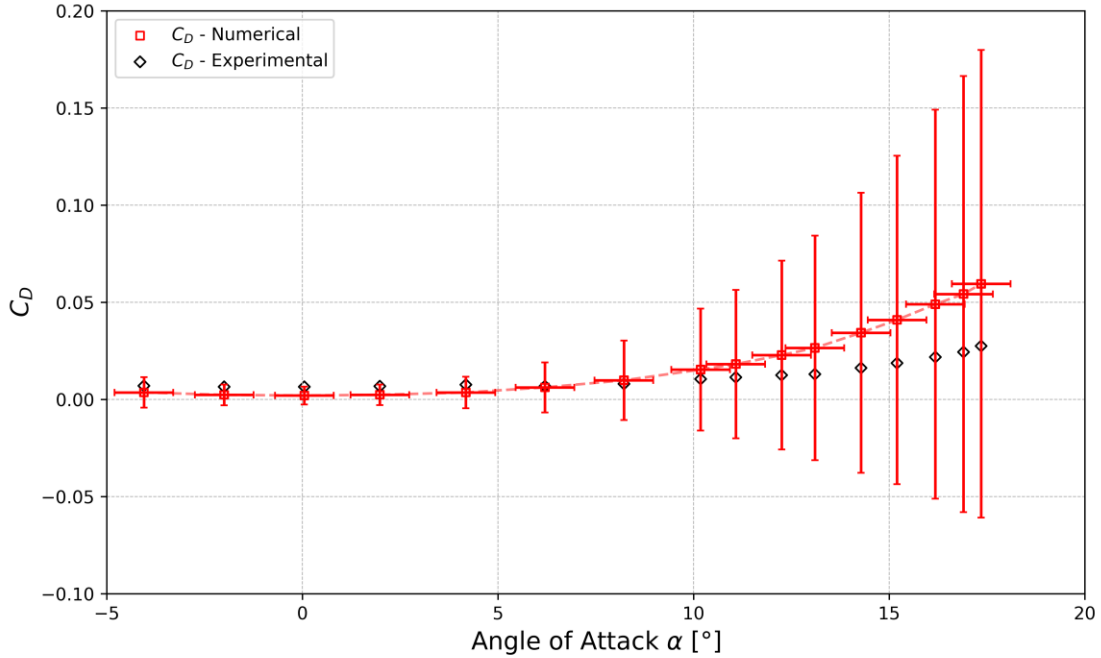

MODEL ERROR – δ_{model}

Finally, model error can be found with uncertainties at a standard deviation away from the comparison error, where k = 2:

$$\delta_{model} \epsilon [E - ku_{val}, E + ku_{val}]$$

- Where the validation uncertainty is defined as:

$$u_{val} = \sqrt{u_{input}^2 + u_{num}^2 + u_D^2}$$

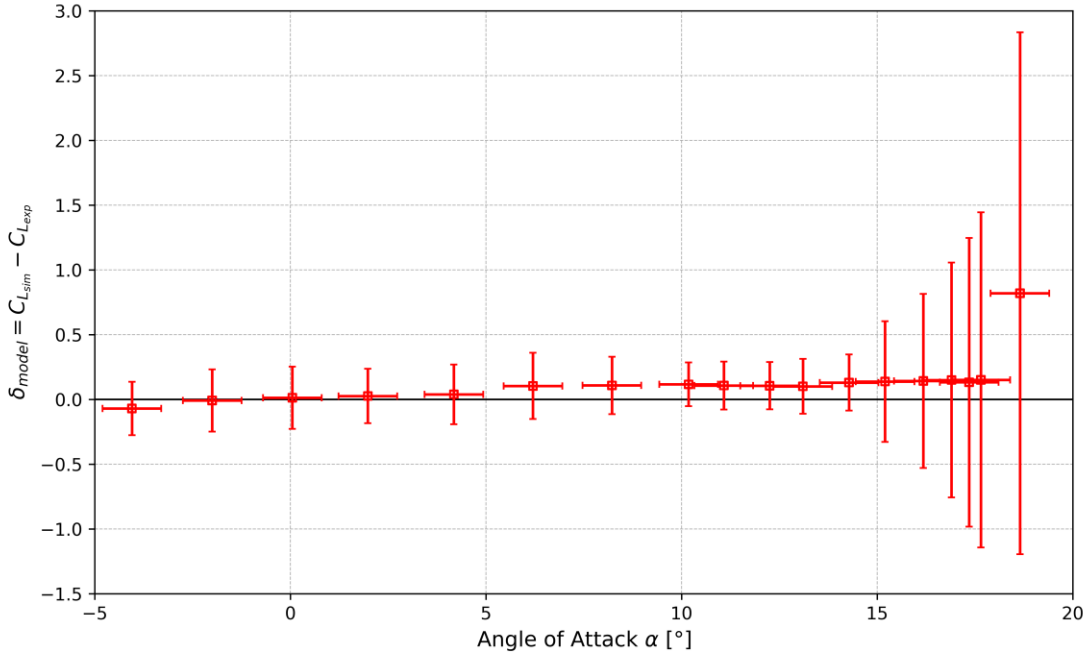

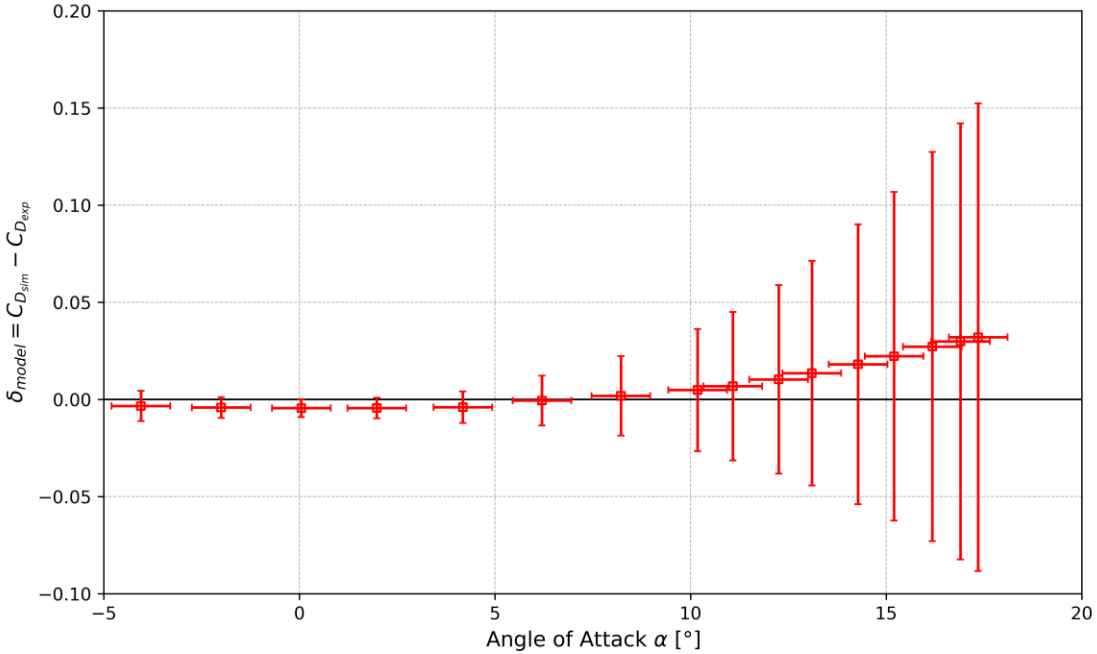

CONTINUED: MODEL ERROR – δ_{model}

Undesirable outcomes are seen across all setpoints for both SRQs. The validation uncertainty is seen to be larger than the comparison error for all setpoints. For the pre-stall setpoints, this can mostly be attributed to lack of rigor on the part of the experimentalist (in reality, it is due to the arbitrarily chosen, hyper-conservative, normal distribution of the input parameters. For example, in hindsight, σ = 0.75° for angle of attack is very extreme). This would have been prevented however, if the Ladson 1988 experimental text contained explicit uncertainties for their experiments' inputs. For the post-stall setpoints, the large uncertainty can be mostly attributed to numerical uncertainty, where stall is not seen to be captured the same way across grid sizes, leading to an observed order of convergence which greatly differs from the formal order of the utilized Roe scheme.

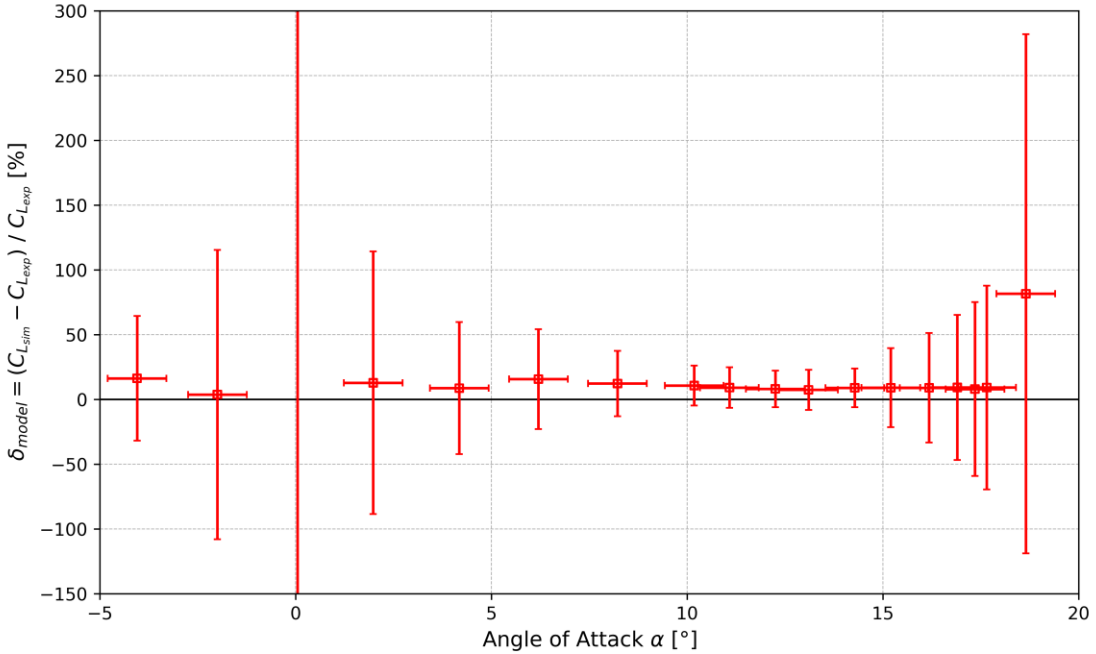

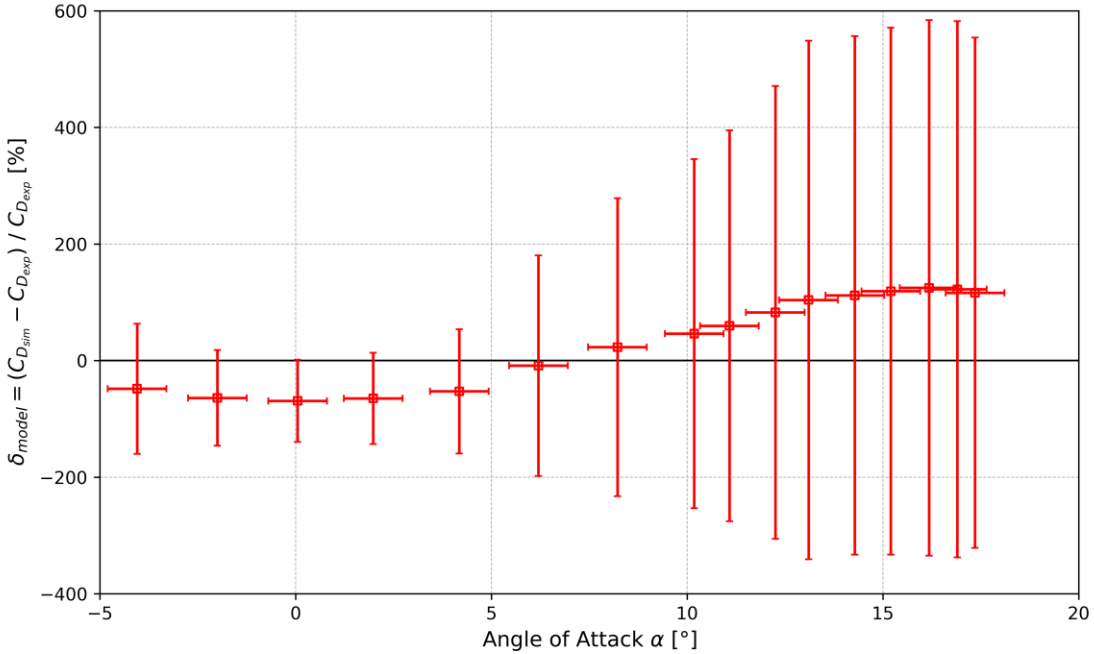

CONTINUED: MODEL ERROR – δ_{model}

While inconclusive, valuable information can still be extracted from the validation procedure. For certain **setpoints**, the sign of the model error can almost be inferred, where E is almost larger than u_{val}. For other **setpoints**, all that can be inferred is the upper limit of the magnitude of δ_{model} model error , given that $u_{val} >> |E|$.

The validation procedure would have a more desirable outcome if the following issues could be remedied: propagated input uncertainties with extremely large distributions and differences in capture of stall across grid sizes resulting in large numerical uncertainty.

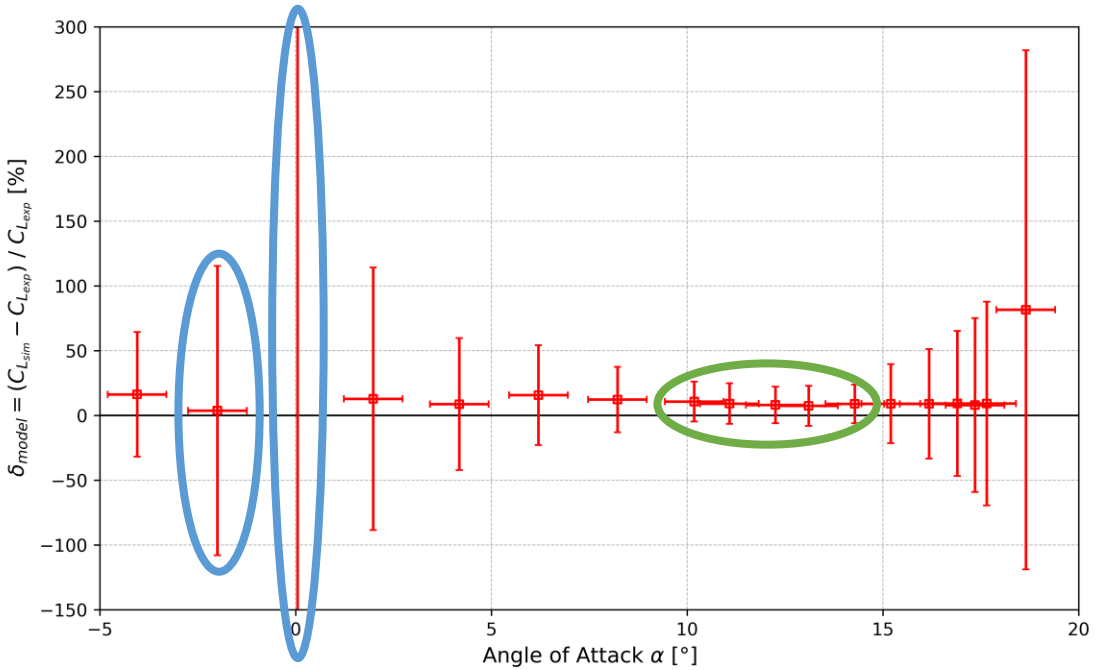

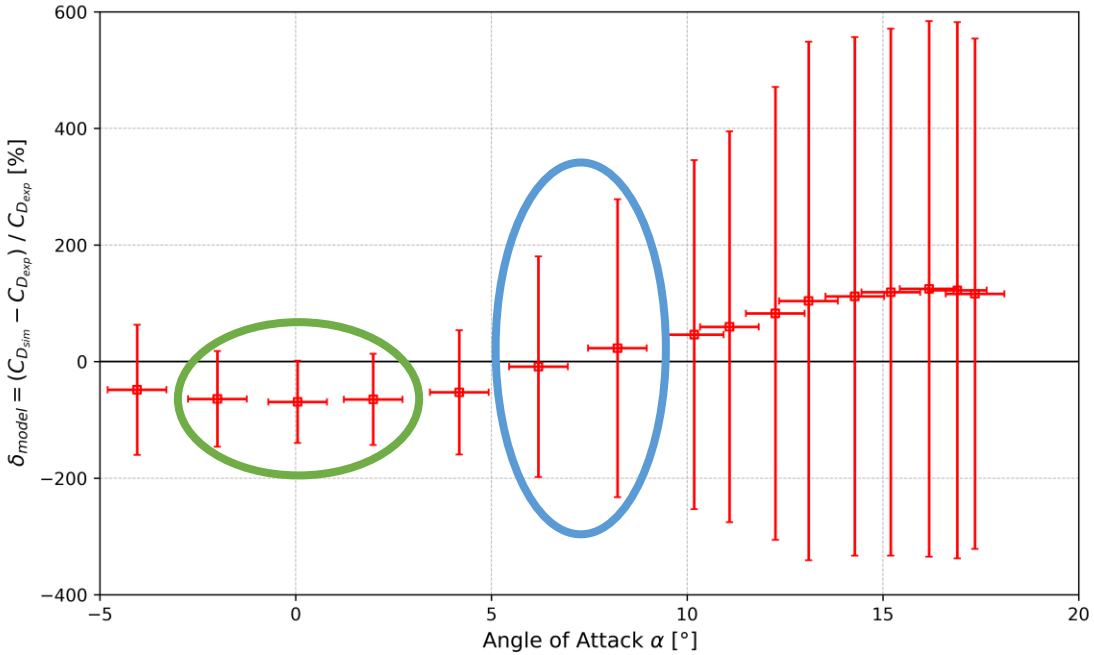

SYNOPSIS

Comparison error and numerical uncertainty increase in function of the setpoint angle of attack. Strangely, the input uncertainty is seen to respectively decrease and increase for C_L and C_D in function of the setpoint angle of attack. This demonstrates that the C_D SRQ is more sensitive to changes in inputs than the C_L SRQ. Overall, it is evident that the greatest source of uncertainty is numerical for both C_L and C_D SRQs.

The usage of a 1st – order spatial scheme can be a possible explanation to the large numerical uncertainty. Typically, 1st – order schemes exhibit a lot of dissipation which may have caused the difficulties seen in capturing stall across grid sizes. Conversely, 2nd – order accurate schemes result in less dissipation and more dispersion, a trade-off which can be beneficial in the capture of stall phenomena. The Roe + MUSCL scheme or the JST scheme would most likely lead to a lower numerical uncertainty. Nevertheless, the conducted validation procedure demonstrates that the 1st – order Roe scheme cannot be relied upon with certainty within a confidence interval of 95.4% for this case's flow conditions.

C_L

α [°]	D	S	E	u_{num}	u_{input}	u_D	u_{val}
-4.05	-4.280e-1	-4.978e-1	-6.981e-2	2.560e-3	1.028e-1	4.000e-3	1.029e-1
-2.00	-2.150e-1	-2.230e-1	-8.003e-3	5.599e-3	1.199e-1	4.000e-3	1.201e-1
0.05	4.000e-3	1.713e-2	1.313e-2	9.129e-6	1.202e-1	4.000e-3	1.203e-1
1.98	2.080e-1	2.347e-1	2.669e-2	9.178e-4	1.054e-1	4.000e-3	1.054e-1
4.18	4.520e-1	4.914e-1	3.943e-2	2.822e-3	1.150e-1	4.000e-3	1.151e-1
6.20	6.630e-1	7.671e-1	1.041e-1	5.582e-3	1.276e-1	4.000e-3	1.278e-1
8.22	8.800e-1	9.880e-1	1.080e-1	1.066e-2	1.105e-1	4.000e-3	1.110e-1
10.18	1.088e+0	1.204e+0	1.165e-1	1.907e-2	8.195e-2	4.000e-3	8.423e-2
11.08	1.180e+0	1.288e+0	1.076e-1	2.462e-2	8.898e-2	4.000e-3	9.241e-2
12.25	1.292e+0	1.398e+0	1.057e-1	0.000e+0	9.118e-2	4.000e-3	9.127e-2
13.10	1.368e+0	1.469e+0	1.012e-1	4.273e-2	9.697e-2	4.000e-3	1.060e-1
14.28	1.458e+0	1.589e+0	1.306e-1	5.831e-2	9.154e-2	4.000e-3	1.086e-1
15.20	1.528e+0	1.666e+0	1.382e-1	2.243e-1	6.258e-2	4.000e-3	2.329e-1
16.18	1.590e+0	1.733e+0	1.429e-1	3.301e-1	6.344e-2	4.000e-3	3.362e-1
16.90	1.618e+0	1.768e+0	1.497e-1	4.508e-1	4.604e-2	4.000e-3	4.532e-1
17.35	1.660e+0	1.793e+0	1.328e-1	5.557e-1	4.002e-2	4.000e-3	5.572e-1
17.65	1.645e+0	1.796e+0	1.510e-1	6.457e-1	3.807e-2	4.000e-3	6.468e-1
18.65	1.005e+0	1.825e+0	8.198e-1	1.007e+0	3.138e-2	4.000e-3	1.007e+0

C_D

α [°]	D	S	E	u_{num}	u_{input}	u_D	u_{val}
-4.05	7.000e-3	3.619e-3	-3.381e-3	3.827e-3	7.622e-4	2.000e-4	3.907e-3
-2.00	6.500e-3	2.340e-3	-4.160e-3	2.637e-3	3.710e-4	2.000e-4	2.670e-3
0.05	6.500e-3	2.014e-3	-4.486e-3	2.279e-3	1.302e-4	2.000e-4	2.292e-3
1.98	6.800e-3	2.394e-3	-4.406e-3	2.626e-3	3.675e-4	2.000e-4	2.659e-3
4.18	7.600e-3	3.593e-3	-4.007e-3	3.949e-3	8.707e-4	2.000e-4	4.049e-3
6.20	6.800e-3	6.207e-3	-5.929e-4	6.243e-3	1.552e-3	2.000e-4	6.436e-3
8.22	8.000e-3	9.842e-3	1.842e-3	1.000e-2	2.128e-3	2.000e-4	1.023e-2
10.18	1.050e-2	1.536e-2	4.861e-3	1.551e-2	2.517e-3	2.000e-4	1.572e-2
11.08	1.140e-2	1.821e-2	6.809e-3	1.880e-2	3.381e-3	2.000e-4	1.911e-2
12.25	1.250e-2	2.283e-2	1.033e-2	2.392e-2	4.180e-3	2.000e-4	2.429e-2
13.10	1.300e-2	2.653e-2	1.353e-2	2.830e-2	5.931e-3	2.000e-4	2.892e-2
14.28	1.620e-2	3.432e-2	1.812e-2	3.538e-2	6.779e-3	2.000e-4	3.603e-2
15.20	1.870e-2	4.095e-2	2.225e-2	4.176e-2	6.529e-3	2.000e-4	4.227e-2
16.18	2.180e-2	4.900e-2	2.720e-2	4.940e-2	8.130e-3	2.000e-4	5.007e-2
16.90	2.440e-2	5.424e-2	2.984e-2	5.551e-2	8.288e-3	2.000e-4	5.612e-2
17.35	2.750e-2	5.951e-2	3.201e-2	5.954e-2	8.691e-3	2.000e-4	6.017e-2

THANK YOU!

POLYTECHNIQUE
MONTRÉAL